



# Environmental changes in Hunshandake (Otindag) sandy land revealed by optical dating and multi-proxy study of dune sands



Zhijun Gong<sup>a,b</sup>, Sheng-Hua Li<sup>b,\*</sup>, Jimin Sun<sup>a</sup>, Lei Xue<sup>c</sup>

<sup>a</sup> Institute of Geology and Geophysics, Chinese Academy of Sciences, P.O. Box 9825, Beijing 100029, China

<sup>b</sup> Department of Earth Sciences, The University of Hong Kong, Pokfulam Road, Hong Kong, China

<sup>c</sup> Xiamen Seismological Survey and Research Center, Xiamen, China

## ARTICLE INFO

### Article history:

Received 13 July 2012

Received in revised form 18 July 2013

Accepted 24 July 2013

Available online 6 August 2013

### Keywords:

OSL dating

Hunshandake (Otindag) sandy land

Paleoclimate

East Asian monsoon

## ABSTRACT

A stabilized sand dune from the southern Hunshandake (Otindag) sandy land in northeastern China was studied for reconstructing past environmental changes by optically stimulated luminescence (OSL) dating, magnetic susceptibility and particle size analysis. The OSL dating results indicate that the sandy deposits at the bottom of the section formed at  $\sim 11.8$  ka ago, corresponding to low magnetic susceptibility and low fractions of fine particles ( $< 63 \mu\text{m}$ ). The variations of the two climate proxies suggest that the region was mainly influenced by arid climate. Above the bottom sand layer, there are loamy soils, which formed between  $\sim 6.2$  and  $\sim 4.3$  ka ago. The soils have relatively higher magnetic susceptibility and finer grain size than the bottom sands. The climate of this period was relatively warm and humid, dominated by enhanced summer monsoon. During the late Holocene (from  $\sim 4$  ka to present), Hunshandake was dominated by semi-humid to arid climate, as indicated by the aeolian sand beds and interbedded weak sandy soils.

© 2013 Elsevier Ltd. All rights reserved.

## 1. Introduction

In arid and semi-arid regions, aeolian deposits are important geologic archives for reconstructing paleoenvironment. Active sand dunes are widely distributed in sandy lands in northeastern China. Most of these deserts have relict sand dunes, characterized by alternating units of paleosols and sands. These alternative units can be used as evidence for past environmental change during the late Quaternary. Hunshandake (Otindag) sandy land is located at the northern limit of East Asian monsoon zone in China (Fig. 1). The variations in the strength of East Asian monsoon may have significant impacts on the advance and retreat of the desert during the geologic past (Mason et al., 2009; Sun et al., 1998).

Several chronological studies have been carried out in the desert and the adjacent areas, using radiocarbon dating and optically stimulated luminescence (OSL) dating methods (Li et al., 2002; Chen et al., 2003; Han and Sun, 2004; Jin et al., 2004; Zhou et al., 2008). For radiocarbon dating, only a few sporadic sections were dated due to the lack of adequate organic material in such semi-arid/arid areas. For many sandy aeolian depositional sequences, the OSL dating has provided a reliable chronology. This technique has been applied widely to the relict sand dunes from northeastern China (Li et al., 2002; Sun et al., 2006; Li et al., 2007; Zhao et al.,

2007; Zhou et al., 2008). In this study, a representative sand dune from the southern Hunshandake sandy land was investigated by using OSL dating and climatic proxies. Sedimentary sequences in this dune field mainly reflect changes of the dune system and variations of climate. Thus, they provide an important example for Holocene paleoenvironmental changes in a fragile ecosystem region influenced by regional scale East Asian monsoons.

## 2. Geological setting

The Hunshandake sandy land occupies an area of  $\sim 52,000 \text{ km}^2$ , with an average elevation of 1100 m. Dunes are mostly semi-stabilized to stabilized, and the most common vegetations are *Poaceae*, *Artemisia*, *Salix microstachya*, and trees like *Ulmus*. The dune field of the Hunshandake sandy land extends from northwest to southeast, with heights range from 10 to 30 m. Stabilized linear dunes mainly occur in the northwest, while parabolic to barchan dunes distribute in the southeast (Fig. 1).

Hunshandake sandy land is affected by the East Asian monsoon circulation (Fig. 1). In summer, the prevailing southeasterly wind brings humid air masses from the Pacific Ocean. In contrast, the dominant wind in winter is northwesterly and frequent dust storms usually occur in spring (Li et al., 2002). The annual precipitation is between 200 mm and 400 mm. About 80–90% of precipitation falls between August and September. The precipitation also shows spatial differences in the region. The annual precipitation in

\* Corresponding author. Tel.: +86 22415486.

E-mail address: [shli@hku.hk](mailto:shli@hku.hk) (S.-H. Li).

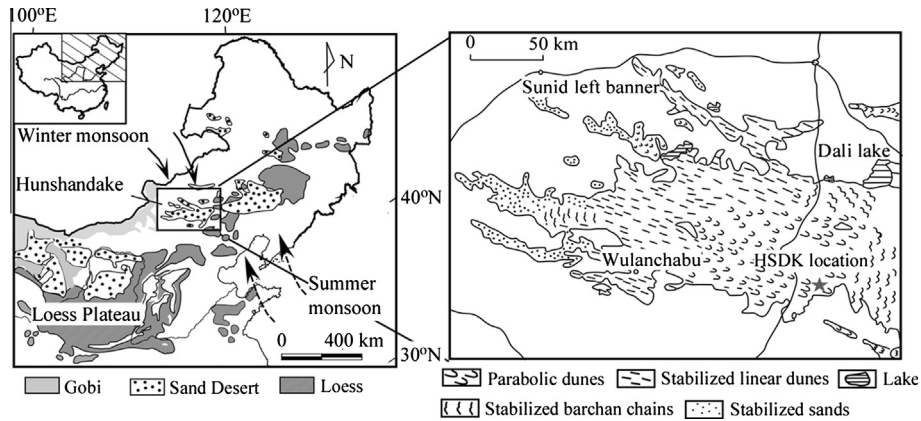


Fig. 1. Map showing Hunshandake Desert and the studied section location (the right graph was modified from (Zhu et al., 1980)).

the southeast part can reach 350 mm and even 400 mm, while it is only 200 mm or less in the northwest part (Chen et al., 2009).

The studied section is situated at the southern edge of Hunshandake sandy land (N42°39'27.2", E115°57'3.0"). The section is a relict stabilized barchan dune, about 9.0 m in height and covered by sparse vegetation (Fig. 2). The lithology of this section is dominated by light yellow (10YR, 8/4) sand and light brownish gray (7.5YR, 7/1) sandy soil, but with an interbedded dark brown (7.5YR, 3/3) sandy loamy soil in its lower part. Detailed observations indicate that it is an initial stage soil, showing only humus accumulation (A) horizon based on the soil diagnostic features of a soil pedon (Harden,1982).

### 3. Methods

#### 3.1. Sample collection and optical dating

The OSL dating samples were obtained by hammering stainless steel tube into the freshly cleaned vertical section. These tubes were covered with a lid soon after taking them from the section, then sealed in black plastic bag. A total of 11 samples were col-

lected for OSL dating. Ninety bulk samples were also taken from the section with a sampling interval of 10 cm. These samples were collected to study the magnetic susceptibility and particle size, as proxies for past climate changes.

The OSL dating samples were studied in Luminescence Dating Laboratory, The University of Hong Kong. The material at the each end of the tube was scraped away and used for dose rate measurements. Raw samples in centre of the tube were treated with 10% hydrochloric acid (HCl) and 10% hydrogen peroxide (H<sub>2</sub>O<sub>2</sub>) to remove carbonates and organic materials, respectively. These samples were then prepared following the procedures: dry sieving, heavy liquid separation and hydrofluoric acid (HF) etching in subdued red safe light conditions (Li et al. 2007). Grains between 180 and 212 μm were selected by mechanical dry sieving. Potassium-feldspar (K-feldspar) grains and quartz grains were separated using sodium polytungstate heavy liquid (2.58 g/cm<sup>3</sup> for K-feldspar, 2.75 g/cm<sup>3</sup> for quartz). The K-feldspar grains were etched with 10% HF for 30 min to remove the outer alpha dosed layer; while the quartz grains were etched with 40% HF for 80 min to remove the outer alpha dosed layer as well as any remaining feldspar. HCl (10%) was then used again to dissolve any residual fluorides

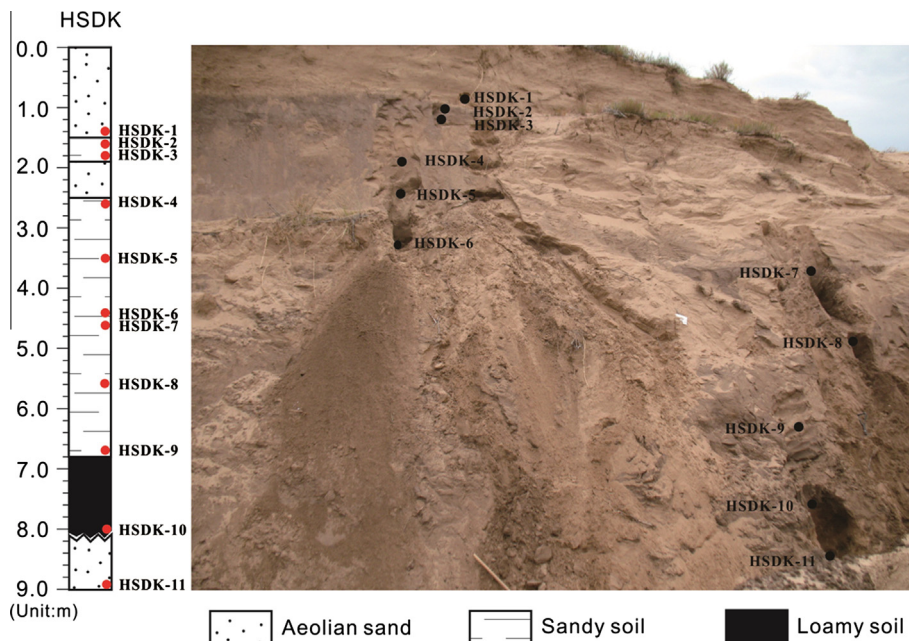


Fig. 2. A stratigraphic section of a representative stabilized dune from southern part of Hunshandake sandy land.

after etching before final rinsing and drying. Aliquots containing several hundred grains were prepared by mounting the grains in a monolayer on a 9.8 mm diameter aluminum disc with “silko-spray” silicone oil for OSL measurement. The purity of quartz grains was tested by monitoring the presence of feldspar by measuring the infrared stimulated luminescence (IRSL) and 110 °C thermal luminescence (TL) peak (Li et al., 2002).

OSL signals were measured using automated Risø TL/OSL readers equipped with excitation units of blue light (BL 470 Δ 20 nm) and infrared light (IR 870 Δ 40 nm). The IR and BL stimulations deliver ~135 mW/cm<sup>2</sup> and ~50 mW/cm<sup>2</sup> at the sample, respectively (Bøtter-Jensen et al., 2003). 90% of their full powers were used for stimulation in this study. The quartz OSL signals were detected through 7.5 mm Hoya U-340 filters, which mainly pass light from 290 nm to 370 nm with peak transmission at ~340 nm (Aitken, 1998). The IRSL signals from K-feldspar were detected through a filter pack containing Schott BG-39 and Corning 7–59 filters, which allows for a transmission peak in blue (320–480 nm). Irradiation was carried out using <sup>90</sup>Sr/<sup>90</sup>Y beta sources built into the readers.

The equivalent doses ( $D_e$ ) of quartz were determined by the single-aliquot regenerative-dose (SAR) protocol (Wintle and Murray, 2006). In the protocol, the preheating condition was tested for sample HSDK-11 from 180 °C to 300 °C in steps of 20 °C (Fig. 3). Based on the test, we selected preheating temperature at 260 °C for 10 s and cut-heat at 220 °C before the regenerative dose and test dose OSL measurement, respectively. Aliquots with recycling ratio falling out the range of  $1.0 \pm 0.1$  were removed for age calculation. More than 20 aliquots were used for each sample.

Potassium rich feldspar (K-feldspar) grains can also be used for dating of sediments. K-feldspar has advantages of bright luminescence and homogeneous  $D_e$  results over quartz. Recently, the multi-elevated-temperature post IR IRSL (MET-pIRIR) protocol was proposed to overcome the problem of anomalous fading (Li and Li, 2011). In such protocol, it measures the IRSL signals from K-feldspar by progressively increasing the IR stimulation temperature from 50 °C to 250 °C in steps of 50 °C. These IRSL signals at different stimulation temperatures were termed as the MET-pIRIR signals. Good performance of the protocol has been reported for its use of dating aeolian sedimentary samples from deserts in northern China and loess samples from Chinese Loess Plateau. In this study, the MET-pIRIR protocol was applied to sample HSDK-11 for cross-checking. In the MET-pIRIR protocol, preheating at 280 °C for 10 s was used for both the regenerative dose and test dose IRSL measurements. Eight aliquots were measured for K-feldspar grains of sample HSDK-11.

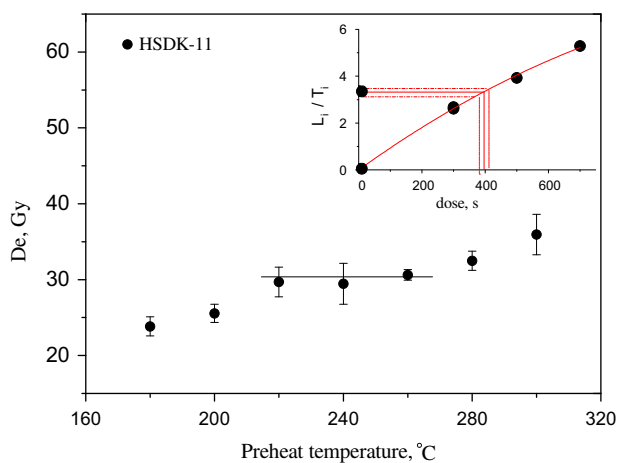


Fig. 3. Measured equivalent dose versus preheat temperature for sample HSDK-11. At least 4 aliquots per temperature were used. The horizontal line denotes that the preheat plateau were reached from 220 °C to 260 °C.

The dose rate was measured using thick source alpha counting and flame photometry. Thick source alpha counting was used to measure contributions to dose rate from the Uranium (U) and Thorium (Th) decay chains. The alpha count rates were converted into alpha, beta and gamma dose rate (Aitken, 1985). Potassium content was measured by flame photometry. Water content was the ratio of water weight to the dried sample weight, obtained from the sample weights before and after drying at 105 °C in an oven. The cosmic ray contribution to the dose rate was calculated from the burial depth, latitude, longitude and altitude of the samples (Prescott and Hutton, 1994). The internal dose rate for K-feldspar was calculated using a potassium concentration of  $13 \pm 1\%$  and a Rb concentration of  $400 \pm 100 \mu\text{g/g}$ , using published absorbed beta dose fractions for spherical grains (Huntley and Baril, 1997; Zhao and Li, 2005; Li et al., 2008).

### 3.2. Magnetic susceptibility and particle size

Magnetic susceptibility analysis was conducted using a Bartington M.S.2 instrument in the Geomagnetism Laboratory in Institute of Geology and Geophysics, Chinese Academy of Sciences. Particle size was measured in Sedimentology/Wet Chemistry Laboratory, The University of Hong Kong. The samples were pretreated according to procedures, as described in elsewhere (Konert and Vandenberghe, 1997; Li et al., 2012). In preparation, the carbonate and organic materials were removed by HCl and H<sub>2</sub>O<sub>2</sub>, respectively. The samples were also added in 0.05 mol/L (NaPO<sub>3</sub>)<sub>6</sub> and then shaken in an ultrasonic machine for 10 min, in order to avoid any aggregation of the individual grains. Finally, the samples were measured by the Ls 13 320 (BECKMAN COULTER) Laser Diffraction Particle Size Analyzer.

## 4. Results

### 4.1. Optical dating

The OSL dating results for quartz grains are summarized in Table 1. The quartz samples from the section show similar luminescence characteristics. Fig. 4 shows representative  $D_e$  results from one of these samples (HSDK-11). The normal distribution of  $D_e$  results in histogram, together with the results from Radial plot, suggests that the grains were well bleached prior to deposition (the over-dispersion value is 7% for the sample). Our quartz OSL ages of this section range are from  $11.8 \pm 0.8$  ka to  $2.06 \pm 0.16$  ka. To test the reliability of the quartz OSL ages, K-feldspar grains from sample HSDK-11 were also dated with the MET-pIRIR protocol (Li and Li, 2011). The details of  $D_e$ , dose rate and IRSL ages for K-feldspar from sample HSDK-11 are shown in Table 2. Homogeneous  $D_e$  values were obtained from the K-feldspar aliquots. Fig. 5 shows the age plateau from 150 °C to 250 °C in the MET-pIRIR age plot. The age plateau has an agreement with the quartz OSL age. The results of the age plateau in MET-pIRIR age plot support the determination that the samples were well bleached before deposition, since K-feldspar IRSL signals were bleached slower than quartz OSL signals (Godfrey-Smith et al., 1988). The consistence of the quartz age with the K-feldspar ages from sample HSDK-11 provides a cross check on the reliability of these dates.

### 4.2. Climatic proxy indices – magnetic susceptibility and particle size

Magnetic susceptibility has been widely used in loess sequence as a climatic proxy of East Asia summer monsoon intensity (An et al., 1991; Zhou et al., 1990). A strong correlation was demonstrated between magnetic susceptibility record of Chinese loess and oxygen isotope record of deep-sea cores. Magnetic susceptibil-

**Table 1**  
Results of quartz equivalent dose, dose rate and OSL ages for samples from Hunshandake (Otindag) sandy land.

Sample	Depth (m)	Alpha counting rate <sup>a</sup>	K content (%)	Water content <sup>b</sup> (%)	Cosmic ray <sup>c</sup> (Gy/Ka)	De (Gy)	Dose rate (Gy/ka)	OSL age (ka)
HSDK-1	1.4	2.53 ± 0.10	2.41 ± 0.24	2.6	0.21	5.8 ± 0.3	2.83 ± 0.18	2.06 ± 0.16
HSDK-2	1.6	3.57 ± 0.12	2.41 ± 0.24	3.1	0.21	7.7 ± 0.3	2.96 ± 0.18	2.61 ± 0.20
HSDK-3	1.8	2.40 ± 0.09	2.41 ± 0.24	2.7	0.20	8.7 ± 0.3	2.80 ± 0.18	3.13 ± 0.23
HSDK-4	2.6	3.15 ± 0.10	2.28 ± 0.23	3.1	0.19	8.2 ± 0.4	2.76 ± 0.18	2.96 ± 0.23
HSDK-5	3.5	2.91 ± 0.10	2.28 ± 0.23	5.9	0.16	8.6 ± 0.4	2.62 ± 0.17	3.30 ± 0.26
HSDK-6	4.4	2.72 ± 0.09	2.28 ± 0.23	4.9	0.14	10.3 ± 0.6	2.60 ± 0.17	3.92 ± 0.32
HSDK-7	4.6	3.54 ± 0.10	2.28 ± 0.23	11.3	0.14	9.9 ± 0.5	2.53 ± 0.16	3.93 ± 0.31
HSDK-8	5.6	2.89 ± 0.10	2.28 ± 0.23	6.7	0.13	9.3 ± 0.5	2.56 ± 0.17	3.75 ± 0.32
HSDK-9	6.7	3.68 ± 0.11	2.32 ± 0.23	5.3	0.11	11.8 ± 0.7	2.73 ± 0.17	4.33 ± 0.36
HSDK-10	8.0	3.92 ± 0.10	2.32 ± 0.23	5.1	0.10	17.0 ± 0.7	2.74 ± 0.17	6.19 ± 0.47
HSDK-11	9.0	1.96 ± 0.09	2.32 ± 0.23	1.0	0.09	30.6 ± 0.7	2.59 ± 0.17	11.8 ± 0.8

<sup>a</sup> The alpha counting rate is for a 42-mm-diameter ZnS screen and is given in units of counts per 1000 s.

<sup>b</sup> The error for the water content is estimated at ±20%.

<sup>c</sup> The error for the cosmic rays dose rate is estimated at ±0.02 Gy/ka.

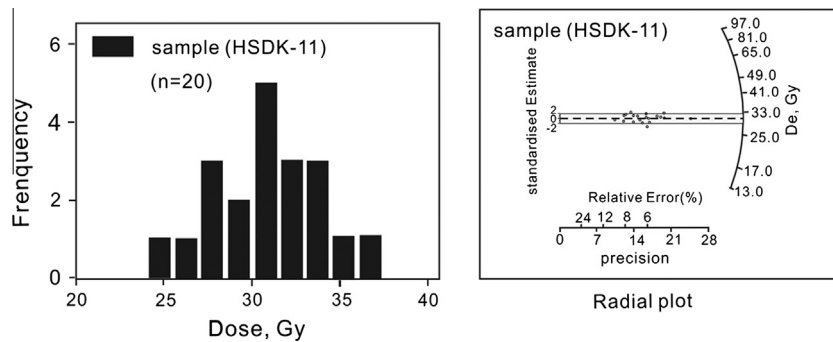


**Fig. 4.** Histograms and radial plot of De distribution for sample HSDK-11. The dashed area indicates the ±2σ standard error band. The over-dispersion value is 7% for the sample.

**Table 2**  
Equivalent dose, dose rate and IRSL ages for K-feldspar from sample HSDK-11, measured with the MET-pIRIR protocol.

IR stimulation temperatures used in MET-pIRIR protocol	50 °C	100 °C	150 °C	200 °C	250 °C
De (Gy)	29.4 ± 0.5	34.7 ± 0.3	38.9 ± 0.6	42.2 ± 0.7	42.6 ± 0.4
Dose rate (Gy/ka)	3.44 ± 0.19	3.44 ± 0.19	3.44 ± 0.19	3.44 ± 0.19	3.44 ± 0.19
Age (Ka)	8.6 ± 0.5	10.1 ± 0.6	11.3 ± 0.6	12.3 ± 0.7	12.4 ± 0.7

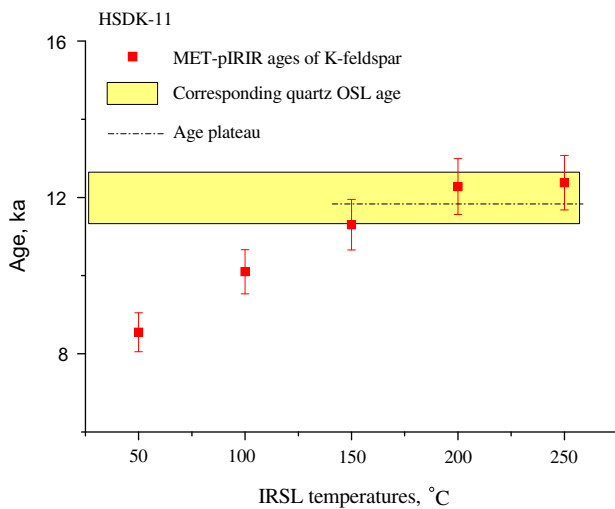


**Fig. 5.** The IRSL ages of K-feldspar for sample HSDK-11, using the MET-pIRIR protocol. The yellow shaded area in the plot showed the corresponding quartz OSL age.

ity was also used as climate proxy to study the environment changes in Hobq Desert, Mu Us Desert and Gurbantunggut Desert (Sun et al., 2006; Li and Fan, 2011). A prevailing interpretation is

that the enhanced magnetic susceptibility in paleosol is due to the newly formed ultrafine magnetite minerals (e.g., Zhou et al., 1990). Therefore, the weathered deposits formed in warm and humid phase have higher magnetic susceptibility. In the HSDK section, the highest magnetic susceptibility values are observed in the loamy soil layer at the depth of 6.8–8.1 m (Fig. 6), while the lowest susceptibility values correspond to a sand layer at the depth of 0.1–1.2 m of the section.

Particle size of aeolian deposits is another widely used climatic proxy of East Asia winter monsoon intensity (e.g., Ding et al., 1992; Pye and Zhou, 1989; Sun et al., 2006; Vandenberghe et al., 1997; Xiao et al., 1995). In this study, the size fraction (<63 μm) was selected as the proxy for inferring winter monsoon strength (Lu et al., 1999). The variations of particle size of HSDK section are shown in Fig. 6. It shows that the sandy layers have lower size fraction of <63 μm compared with that of the loamy soils.

## 5. Discussion

Hunshandake Desert is situated at the present northern limit of East Asian monsoon in China. The past variations in the strength of East Asian monsoon had effects on the activity of sand dunes in the sandy land (Li et al., 2002; Lu et al., 2005). When the summer monsoon circulation was enhanced, it led to increasing precipitation and warm climate, being favorable for vegetation growth and sand dune stabilization. When the winter monsoon circulation was

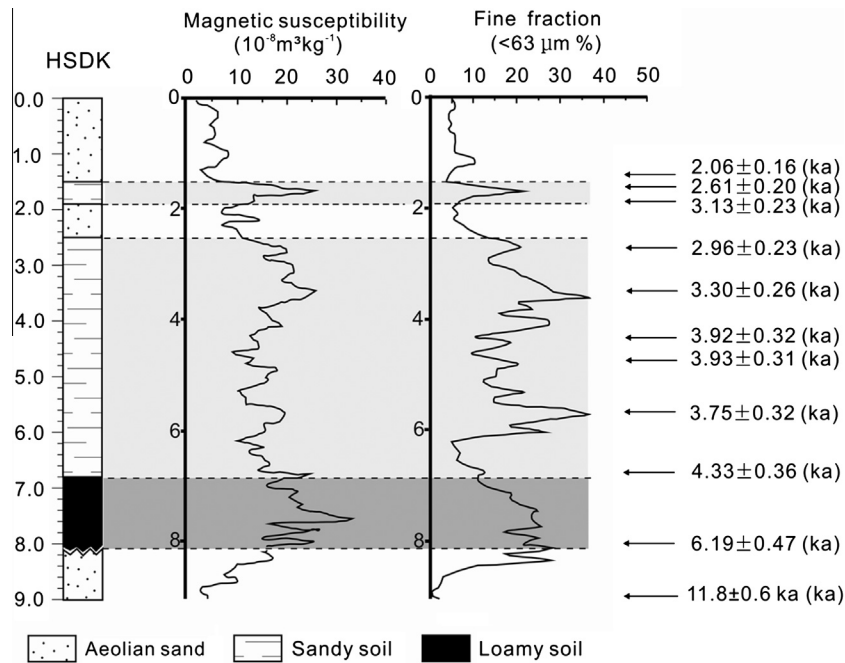


Fig. 6. Stratigraphy, magnetic susceptibility and particle size variations of the HSDK section from Hunshandake Desert.

intensified, this sandy field was influenced by cold/dry climate, leading to the mobilization of sand dunes due to the reduction of vegetation cover (Li and Sun, 2006).

Using the OSL chronology and climatic proxy indicators, the climatic changes in Hunshandake sandy land were reconstructed for the last 11.8 ka (refer to Fig. 6).

- (1) From the bottom to 8.15 m ( $\sim 11.8$  ka ago). Relative low magnetic susceptibility and low fractions of fine particles of  $<63 \mu\text{m}$  suggest that dry climate prevailed at that time. A hiatus of deposition appeared between the top of this sand layer and the loamy soil layer in the section (Fig. 6).
- (2) From 8.15 m to 6.80 m ( $\sim 6.2$  ka to  $\sim 4.3$  ka ago). Relatively high magnetic susceptibility and higher fine particle fractions are recorded in the loamy soils. The two proxy indicators suggest that the summer monsoon circulation was strong and the winter monsoon circulation was relatively weak. The humid conditions were favorable for the sand dune stabilization and the loamy soil development. This period was partially associated with the Holocene Optimum (Li and Sun, 2006).
- (3) Although a soil development in arid region may also be related to warm and humid climate and the lack of sediment supply, but this latter case is, at least, partially associated with climatic change. For instance, the low particle accumulation in a deposition site is mostly linked to the reduced entrainment and transportation of airborne silt and/or dust in the source region. Moreover, the well-developed humus accumulation (A) horizon indicates quantitative biomass and thus a well-developed vegetation cover during the soil formation. Therefore, this soil is mostly related to the warmer and more humid climate in this region. Additionally, this climate can be correlated with the other previous studies of the same area (Jin et al., 2010; Li et al., 2002).
- (4) From 6.8 m to 2.5 m ( $\sim 4.3$  ka to  $\sim 3$  ka ago). A sandy soil was developed within this interval, suggesting relatively weak summer monsoon strength and a lack of weathering.
- (5) From 2.5 m to the top ( $\sim 3$  ka ago to the present). The deposits are dominated by aeolian sand, intercalated with a weathered sandy soil layer. The relatively low magnetic sus-

ceptibility and low fractions of fine particles suggest that the region was mainly influenced by a much enhanced winter monsoon, except a very short interval at  $\sim 2.6$  ka (Fig. 6). The results indicate that Hunshandake sandy land was generally influenced by cold/arid climate during the last 3 ka.

To better understand past environmental changes in this region, our results were compiled with OSL dating and radiocarbon dating results of other 22 sections at different sites from the Hunshandake sandy land (Li et al., 2002; Han and Sun, 2004; Jin et al., 2004; Lu et al., 2005; Mason et al., 2009; Yang and Yue, 2011; Zhou et al., 2008). Here we plotted the frequency distribution of the different kinds of sediments, against their ages for the last 12 ka (Fig. 7(a)). The frequency is the amount of ages falling within a one thousand year bin (time period) for the three types of sediments: sand, sandy soil and loamy soil, respectively. Sampling bias might influence the results since sands or soils were preferred by the authors in their reported sites. In Fig. 7(a), it is observed that the relative proportions for the sand, sandy soil and loamy soil are different in the 12 bins. In order to have better representative results about the past environmental changes in the region, the sand, sandy soil and loamy soil were given with numbers of “-1”, “0.5” and “1”, respectively. It is to be noted that the loamy soils within the Hunshandake sandy land are very similar, characterized by only the humus accumulation horizon representing a primary soil development stage. If the relative proportion of a certain type of sediment in each bin was taken into account, an index of soil development can be synthesized by summing the weighted values (Fig. 7(b)). If the synthesized index for a bin falls between 0.5 and 1, it suggests that the loamy soil dominates in the region and the region is likely to be mainly influenced by humid/semi-humid climate. If the index falls between 0.5 and  $-0.5$ , it means that the area is likely to be influenced by semi-arid/semi-humid climate. If the index falls between  $-0.5$  and  $-1$ , it means that the region is dominated by the sand deposits and it is likely to be influenced by arid/semi-arid climate. The synthesized index of soil development was shown in Fig. 7(b).

The results suggest that Hunshandake sandy land was influenced by different climate during the past 12 ka. From 12 ka to 8 ka, aeolian sand records were dominant at different sites of Hun-

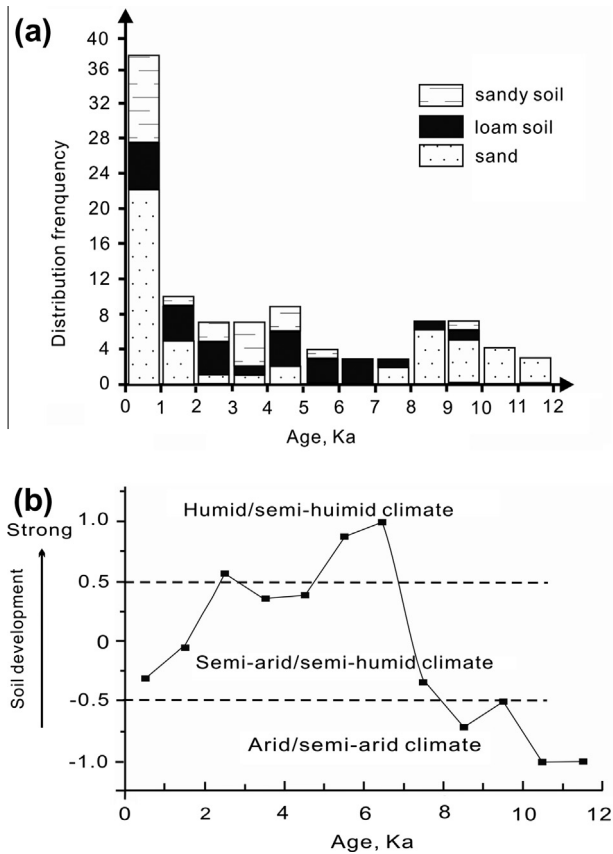


**Fig. 7.** Frequency of different types of sediment, i.e. sand, sandy soil and loamy soil, plotted against their ages for the last 12,000 years. (a) Frequency; (b) climate index (see text).

shandake sandy land. The synthesized index was nearly all below  $-0.5$ , suggesting that the region was mainly influenced by dry climate. Loamy soils were developed between 8 ka and 4 ka. The synthesized index was larger than 0.5 between 5 ka and 7 ka, suggesting that the area was generally influenced by humid/semi-humid climate, being favorable for sand dune stabilization and the loamy soil development. During the late Holocene (i.e. from 4 ka to present), the synthesized index was almost between  $-0.5$  and 0.5, except at  $\sim 2.5$  ka. The results suggest that the area was generally influenced by semi-humid to semi-arid climate.

Therefore, the aeolian deposits in Hunshandake sandy land provide important records for past climate change in the northern China. Similar results were also obtained from sedimentary cores of lakes from mid-high-latitude-monsoon margin in northeastern China, e.g. Daihai Lake, Dali Lake and Hulun Lake (Wen et al., 2010; Xiao et al., 2004; Xiao et al., 2008). Lake-level reconstructions and sedimentary cores from the lakes in the sandy lands in northeastern China suggest that the areas were influenced by different climate during the Holocene. Pollen-assemblage data from sedimentary cores of Hulun Lake and Daihai Lake suggest the dry climate prevailed in the early Holocene and there was a warm and humid phase in the middle Holocene in the areas (Wen et al., 2010; Xiao et al., 2004).

## 6. Conclusion

Hunshandake sandy land was influenced by different climate conditions during the last 12 ka, which was greatly affected by East Asia monsoons. Alternations of sand and soil are response to changes of monsoons. The area was mainly influenced by dry cli-

mate from  $\sim 11.8$  ka to  $\sim 8$  ka. A warm and humid phase was recorded between  $\sim 8$  ka and  $\sim 4$  ka ago in the mid-Holocene as presented as loamy soil development. Semi-humid to arid climate was dominated during the late Holocene.

## Acknowledgement

This study is financially supported by grants to SHL from the Research Grant Council of the HKSAR, China (Project No. 7035/06P, 7035/07P and 7028/08P).

## References

- Aitken, M.J., 1985. Thermoluminescence Dating. Academic Press, London.
- Aitken, M.J., 1998. An Introduction to Optical Dating. Oxford University Press, Oxford.
- An, Z.S., Kukla, G.J., Porter, S.C., Xiao, J., 1991. Magnetic susceptibility evidence of monsoon variation on the Loess Plateau of central China during the last 130,000 years. *Quaternary Research* 36, 29–36.
- Bøtter-Jensen, L., Andersen, C.E., Duller, G.A.T., Murray, A.S., 2003. Developments in radiation, stimulation and observation facilities in luminescence measurements. *Radiation Measurements* 37, 535–541.
- Chen, C.T.A., Lan, H.C., Lou, J.Y., Chen, Y.C., 2003. The dry Holocene Megathermal in Inner Mongolia. *Palaeogeography, Palaeoclimatology, Palaeoecology* 193, 181–200.
- Chen, Y.F., Gu, Z.Y., Chu, G.Q., Xu, B., Lu, Y.W., Sun, X.H., 2009. Lacustrine sediment record for activities of wind and dust in the Hunshandake Desert during the last 50 years (in Chinese). *Quaternary Sciences* 29, 774–780.
- Ding, Z.L., Rutter, N., Han, J.T., Liu, T.S., 1992. A coupled environmental system formed at about 2.5 Ma in East Asia. *Palaeogeography, Palaeoclimatology, Palaeoecology* 94, 223–242.
- Godfrey-Smith, D.I., Huntley, D.J., Chen, W.H., 1988. Optical dating studies of quartz and feldspar sediment extracts. *Quaternary Science Reviews* 7, 373–380.
- Han, P., Sun, J.M., 2004. Optical dating of dune sands in the Hunshandake Desert (in Chinese). *Quaternary Sciences* 24.
- Harden, J.W., 1982. A quantitative index of soil development from field descriptions, examples from a chronosequence in Central California. *Geoderma* 28, 1–28.
- Huntley, D.J., Baril, M.R., 1997. The K content of the K-feldspars being measured in optical dating or in thermoluminescence dating. *Ancient TL* 15, 11–12.
- Jin, H.L., Su, Z.Z., Sun, L.Y., Sun, Z., Zhang, H., Jin, L.Y., 2004. Holocene climatic change in Hunshandake Desert. *Chinese Science Bulletin* 49, 1730–1735.
- Jin, H.L., Sun, L.Y., Sun, Z., 2010. Millennial-scale evolution of Hunshandake Desert and climate change during the Holocene in Inner Mongolia, northern China. *Sciences in Cold and Arid Regions* 2 (6), 505–513.
- Konert, M., Vandenberghe, J., 1997. Comparison of laser grain size analysis with pipette and sieve analysis: a solution for the underestimation of the clay fraction. *Sedimentology* 44, 523–535.
- Li, B., Li, S.-H., 2011. Luminescence dating of K-feldspar from sediments: a protocol without anomalous fading correction. *Quaternary Geochronology* 6, 468–479.
- Li, S.-H., Fan, A.C., 2011. OSL chronology of sand deposits and climate change of last 18 ka in Gurbantungut Desert, northwest China. *Journal of Quaternary Science* 26 (8), 813–818.
- Li, S.-H., Sun, J.M., 2006. Optical dating of Holocene dune sands from the Hulun Buir Desert, northeastern China. *Holocene* 16, 457–462.
- Li, S.-H., Sun, J.M., Zhao, H., 2002. Optical dating of dune sands in the northeastern deserts of China. *Palaeogeography, Palaeoclimatology, Palaeoecology* 181, 419–429.
- Li, S.-H., Chen, Y.Y., Li, B., Sun, J.M., Yang, L.R., 2007. OSL dating of sediments from deserts in northern China. *Quaternary Geochronology* 2, 23–28.
- Li, B., Li, S.-H., Wintle, A.G., Zhao, H., 2008. Isochron dating of sediments using luminescence of K-feldspar grains. *Journal of Geophysical Research-Earth Surface* 113, F02026. <http://dx.doi.org/10.1029/2007JF000900>.
- Li, S.-H., Sun, J.M., Li, B., 2012. Holocene environmental changes in central Inner Mongolia revealed by luminescence dating of sediments from the Sala Us River valley. *The Holocene* 22 (4), 397–404. <http://dx.doi.org/10.1177/0959683611425543>.
- Lu, H.Y., Van Huissteden, K.O., An, Z.S., Nugteren, G., Vandenberghe, J., 1999. East Asia winter monsoon variations on a millennial time-scale before the last glacial-interglacial cycle. *Journal of Quaternary Science* 14, 101–110.
- Lu, H.Y., Miao, X.D., Zhou, Y.L., Mason, J., Swinehart, J., Zhang, J.F., Zhou, L.P., Yi, S.W., 2005. Late Quaternary aeolian activity in the Mu Us and Otindag dune fields (north China) and lagged response to insolation forcing. *Geophysical Research Letters* 32.
- Mason, J.A., Lu, H.Y., Zhou, Y.L., Miao, X.-D., Swinehart, J.B., Liu, Z., Goble, R.J., Yi, S., 2009. Dune mobility and aridity at the desert margin of northern China at a time of peak monsoon strength. *Geology* 37, 947–950.
- Prescott, J.R., Hutton, J.T., 1994. Cosmic-ray contributions to dose-rates for luminescence and Esr dating – large depths and long-term time variations. *Radiation Measurements* 23, 497–500.
- Pye, K., Zhou, L.-P., 1989. Late Pleistocene and Holocene aeolian dust deposition in North China and the Northwest Pacific Ocean. *Palaeogeography, Palaeoclimatology, Palaeoecology* 73, 11–23.

- Sun, J.M., Ding, Z.L., Liu, T.S., 1998. Desert distributions during the glacial maximum and climatic optimum: example of China. *Episodes* 21, 28–31.
- Sun, J.M., Li, S.-H., Han, P., Chen, Y., 2006. Holocene environmental changes in the central Inner Mongolia, based on single-aliquot-quartz optical dating and multi-proxy study of dune sands. *Palaeogeography, Palaeoclimatology, Palaeoecology* 233, 51–62.
- Vandenbergh, J., An, Z.S., Nugteren, G., Lu, H.Y., Huissteden, K.V., 1997. New absolute time scale for the Quaternary climate in the Chinese loess region by grain-size analysis. *Geology* 25, 35–38.
- Wen, R., Xiao, J., Chang, Z., Zhai, D., Xu, Q., Li, Y., Itoh, S., Lomtatidze, Z., 2010. Holocene climate changes in the mid-high-latitude-monsoon margin reflected by the pollen record from Hulun Lake, northeastern Inner Mongolia. *Quaternary Research* 73, 293–303.
- Wintle, A.G., Murray, A.S., 2006. A review of quartz optically stimulated luminescence characteristics and their relevance in single-aliquot regeneration dating protocols. *Radiation Measurements* 41, 369–391.
- Xiao, J., Porter, S.C., An, Z.S., Kumai, H., Yoshikawa, S., 1995. Grain-size of quartz as an indicator of winter monsoon strength on the Loess Plateau of Central China during the last 130,000-Yr. *Quaternary Research* 43, 22–29.
- Xiao, J., Xu, Q., Nakamura, T., Yang, X., Liang, W., Inouchi, Y., 2004. Holocene vegetation variation in the Daihai Lake region of north-central China: a direct indication of the Asian monsoon climatic history. *Quaternary Science Reviews* 23, 1669–1679.
- Xiao, J., Si, B., Zhai, D., Itoh, S., Lomtatidze, Z., 2008. Hydrology of Dali Lake in central-eastern Inner Mongolia and Holocene East Asian monsoon variability. *Journal of Paleolimnology* 40, 519–528.
- Yang, L.R., Yue, L.P., 2011. The environmental transformation from late last glacial to Holocene of Otindag sandyland (in Chinese). *Journal of Earth Environment* 2, 301–306.
- Zhao, H., Li, S.-H., 2005. Internal dose rate to K-feldspar grains from radioactive elements other than potassium. *Radiation Measurements* 40, 84–93.
- Zhao, H., Lu, Y.C., Yin, J.H., 2007. Optical dating of Holocene sand dune activities in the Horqin sand-fields in inner Mongolia, China, using the SAR protocol. *Quaternary Geochronology* 2, 29–33.
- Zhou, L.P., Oldfield, F., Wintle, A.G., Robinson, S.G., Wang, J.T., 1990. Partly pedogenic origin of magnetic variations in Chinese Loess. *Nature* 346, 737–739.
- Zhou, Y.L., Lu, H.Y., Mason, J., Miao, X.D., Swinehart, J., Goble, R., 2008. Optically stimulated luminescence dating of Aeolian sand in the Otindag dune field and Holocene climate change. *Science in China Series D-Earth Sciences* 51, 837–847.
- Zhu, Z.D., Wu, Z., Liu, N., Di, X.M., 1980. *Introduction to Chinese Desert* (in Chinese). Science Press, Beijing.